

Interlayer interactions in $\text{La}_3\text{Ni}_2\text{O}_7$ under pressure: from s^\pm to d_{xy} -wave superconductivity

Lauro B. Braz,¹ George B. Martins,² and Luis G. G. V. Dias da Silva¹

¹*Instituto de Física, Universidade de São Paulo,
Rua do Matão 1371, São Paulo, São Paulo 05508-090, Brazil*

²*Instituto de Física, Universidade Federal de Uberlândia, Uberlândia, Minas Gerais 38400-902, Brazil.*
(Dated: February 13, 2025)

We investigate the role of *interlayer* interaction terms in the competition between different superconducting gap symmetries in the bilayer nickelate $\text{La}_3\text{Ni}_2\text{O}_7$ under high pressure. We study a two-layer, two-orbital electron model that encompasses both intra- and interlayer Coulomb interaction terms within the matrix random-phase approximation. We find that interlayer interactions favor a d_{xy} -wave superconducting pairing symmetry over the s^\pm -wave symmetry, which has been found to prevail when interlayer interactions are disregarded. Moreover, our findings indicate that interlayer interactions enhance the interorbital pairing, incorporating contributions from all three electron pockets, arising from both $d_{3z^2-r^2}$ and $d_{x^2-y^2}$ orbital character, resulting in nodes within the gap function (not present in the s^\pm -wave state) and consequently favoring the d_{xy} -wave pairing.

The recent discovery of high-temperature superconductivity in the Ruddlesden-Popper bilayer nickelate compound $\text{La}_3\text{Ni}_2\text{O}_7$ (LNO327) under high pressure [1–3] has sparked intense research on this new family of high- T_c materials [4]. Despite the rapid progress in the last two years, including recent reports of superconductivity on thin films at ambient pressure [5], several fundamental questions remain on the nature of the underlying pairing mechanism for superconductivity in these compounds.

For example, there has been an intense debate as to which low-energy *minimal* model to describe the superconducting phase. Density Functional Theory calculations [6–9] reveal that multiple bands, mainly formed by Ni-centered in-plane $d_{x^2-y^2}$ and out-of-plane $d_{3z^2-r^2}$ orbitals, along with oxygen-centered p -orbitals cross the Fermi level, forming two electron pockets (α , β) with mixed orbital character and one hole pocket (γ) primarily associated with the Ni- $d_{3z^2-r^2}$ orbital [6]. These bands can be described by a two-layer, two-orbital minimal tight-binding model [6, 7, 9], which has been investigated with interlayer interactions within a localized electron picture [10] and without interlayer interactions in an itinerant electron picture [8, 9, 11–13]. In all cases, RPA calculations suggest that s^\pm -wave pairing is the dominant superconducting instability, driven by intra-orbital (π , 0) scattering between the β and the γ -pockets [8, 9]. However, the d-wave pairing channel is found to have energy close to the s-wave pairing channel [8, 12].

Other works [14, 15] propose a minimal model containing just one of these orbitals (either $d_{x^2-y^2}$ or $d_{3z^2-r^2}$), which predict an s^\pm -wave superconducting gap symmetry, with or without interlayer interactions. In contrast, a proposal of cuprate-like d - p hybridized single orbital brought up the possibility of $d_{x^2-y^2}$ or $d_{x^2-y^2} + is$ superconductivity [16].

On the experimental side, recent explorations of the ambient pressure properties of LNO327 give indications that *interlayer* interactions can be relevant for the superconducting phase at high pressures. Neutron scattering

experiments in polycrystalline samples show evidence of spin excitations in the inelastic channel, which are consistent with strong interlayer exchange couplings [17]. In addition, X-ray absorption measurements [18] revealed dispersive magnons and spin-density wave order patterns which are also consistent with interlayer magnetic exchange being about an order of magnitude larger than intralayer ones. In this work, we investigate the role of the *interlayer* interaction terms in the competition between different superconducting gap symmetries in the system. We consider a two-layer, two-orbital electron model that includes both intra- and interlayer Coulomb interaction terms. Within the matrix random-phase approximation (mRPA) [19–23], we find that interlayer interactions favor a d_{xy} -wave superconductivity over the s^\pm state, which is known to dominate when such interlayer interactions are neglected [8, 11, 14]. Our mRPA calculations reveal that interlayer interactions enhance interorbital pairing involving contributions from *all three* pockets, creating nodes in the gap function (absent in the s^\pm -wave state) and thus favoring the d_{xy} -wave pairing.

Band structure.— In order to describe the (non-interacting) band structure of the system, we consider the four-band low-energy model of Refs. [6, 12]. This tight-binding model involves two orbitals ($d_{x^2-y^2}$ and $d_{3z^2-r^2}$) per Ni atom in a unit cell with two Ni atoms (one for each layer) [as depicted in Fig. 1(a)] and hoppings up to second nearest neighbors. For a valence of 2.5 electrons per Ni atom [24], the resulting Fermi surface and band structure are shown in Fig. 1(b) and (c), respectively, together with the respective Ni orbital contributions.

The FS shows electron pockets α and β with a strong contribution from the $d_{x^2-y^2}$ orbital (red), consistent with ARPES results at ambient pressure [25, 26]. The γ hole pocket at (π, π) , however, is dominated by the $d_{3z^2-r^2}$ orbital (blue) and its presence has been linked to the onset of superconductivity if LNO327 and similar materials [8, 27, 28]. We notice that some of the bands show mixed orbital regions (nearly white) along the $\Gamma - \mathbf{X}$ and

$X - M$ high-symmetry paths [Fig. 1(c)].

Interacting model.— Our model Hamiltonian $H = H_0 + H_I$ involves both the (non-interacting) part described by H_0 as well as an interacting term (H_I) that includes both onsite (U, J) and interlayer (U_\perp, J_\perp) Coulomb and exchange interaction terms, as represented in Fig. 1(a).

The interacting Hamiltonian for the two-orbital itinerant electron model is given by the onsite plus interlayer parts, $H_I = H_{\text{onsite}} + H_{\text{inter}}$, where the onsite term is given by

$$\begin{aligned}
H_{\text{onsite}} = & U \sum_{ij,p\ell} n_{ip\ell\uparrow} n_{ip\ell\downarrow} \\
& + (U' - J/2) \sum_{il,p<q} n_{ip\ell} n_{iq\ell} \\
& - 2J \sum_{il,p<q} \mathbf{S}_{ip\ell} \cdot \mathbf{S}_{iq\ell} \\
& + J \sum_{il,p<q} \left(c_{ip\ell\uparrow}^\dagger c_{ip\ell\downarrow}^\dagger c_{iq\ell\downarrow} c_{iq\ell\uparrow} + \text{h.c.} \right)
\end{aligned} \tag{1}$$

and the interlayer term reads

$$\begin{aligned}
H_{\text{inter}} = & U_\perp \sum_{ij,p\sigma\bar{\sigma}} n_{ipA\sigma} n_{ipB\bar{\sigma}} \\
& + (U'_\perp - J_\perp/2) \sum_{i,p<q} n_{ipA} n_{iqB} \\
& - 2J_\perp \sum_{i,p<q} \mathbf{S}_{ipA} \cdot \mathbf{S}_{iqB} \\
& + J_\perp \sum_{i,p<q} \left(c_{ipA\uparrow}^\dagger c_{ipB\downarrow}^\dagger c_{iqB\downarrow} c_{iqA\uparrow} + \text{h.c.} \right).
\end{aligned} \tag{2}$$

In the above, $c_{ip\ell\sigma}^\dagger$ creates an electron with spin σ , in orbital p , layer $\ell = A, B$, at the (square) lattice site i . In addition, we use a shortcut notation for the density operator, $n_{ip\ell} = \sum_\sigma n_{ip\ell\sigma}$. In the present model, $U(U_\perp)$, $U'(U'_\perp)$, and $J(J_\perp)$ are the onsite (intersite) Hubbard, interorbital, and exchange interaction strengths, respectively.

The interacting part of the Hamiltonian, H_I , can conveniently be rewritten in momentum space as

$$\begin{aligned}
H_I = & \sum_{\mathbf{q}} \sum_{pqstll'} (U_c)^{plq\ell}(\mathbf{q}) n_{plq\ell}(-\mathbf{q}) n_{s\ell't\ell'}(\mathbf{q}) \\
& + \sum_{\mathbf{q}} \sum_{pqstll'} (U_s)^{plq\ell}(\mathbf{q}) \mathbf{S}_{plq\ell}(-\mathbf{q}) \cdot \mathbf{S}_{s\ell't\ell'}(\mathbf{q}),
\end{aligned} \tag{3}$$

where $n_{pAqA}(\mathbf{q}) = \sum_{\mathbf{k}\sigma} c_{(\mathbf{k}+\mathbf{q})pA\sigma}^\dagger c_{\mathbf{k}qA\sigma}$ is the charge density and $\mathbf{S}_{pAqA}(\mathbf{q}) = \sum_{\mathbf{k}\sigma\bar{\sigma}} c_{(\mathbf{k}+\mathbf{q})pA\sigma}^\dagger \boldsymbol{\sigma}_{\sigma\bar{\sigma}} c_{\mathbf{k}qA\bar{\sigma}}$ the spin density for layer A (similarly for layer B), with $\boldsymbol{\sigma}_{\sigma\bar{\sigma}}$ being the Pauli vector. The matrix elements of the charge and spin interaction matrices which connect Eq. (3) with

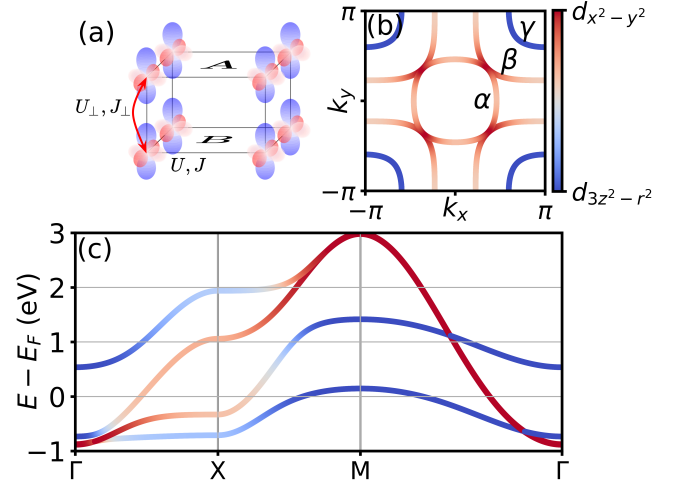


FIG. 1. Schematic representation of the bilayer $\text{La}_3\text{Ni}_2\text{O}_7$ model (a) with onsite U, J and interlayer U_\perp, J_\perp Coulomb and exchange interaction strengths. Fermi surface (b) and band structure (c) for the two-orbital $d_{3z^2-r^2}$ (blue color) and $d_{x^2-y^2}$ (red color) low-energy model.

Eqs. (1) and (2) are given by

$$\begin{aligned}
(U_s)_{pApA}^{pApA} &= U, (U_s)_{qAqA}^{pApA} = U', \\
(U_s)_{pAqA}^{pAqA} &= (U_s)_{qApA}^{pAqA} = J, \\
(U_c)_{pApA}^{pApA} &= U, (U_c)_{qAqA}^{pApA} = (-U' + 2J), \\
(U_c)_{pAqA}^{pAqA} &= J, (U_c)_{qApA}^{pAqA} = (-J + 2U'), \\
(U_c)_{pBpB}^{pApA} &= 2U_\perp, (U_c)_{qBqB}^{pApA} = 2U'_\perp, \\
(U_c)_{pBqB}^{pAqA} &= (U_c)_{qBpB}^{pAqA} = 2J_\perp,
\end{aligned} \tag{4}$$

where A, B denote the respective layer index [29]. For simplicity, we assume spin rotational invariance such that the standard relationship $U' = U - 2J$ holds and we use the usual relation $J = U/4$ and $J_\perp = U_\perp/4$. Notice the interlayer interactions only play a role on the charge interaction channel.

We now consider the singlet-channel RPA pairing interaction matrix [19, 21] for the multi-orbital, multilayer interacting model of Eqs. (3) and (4) [30]:

$$\begin{aligned}
\Gamma_{s\xi t\xi'}^{plq\ell'}(\mathbf{q}) = & \frac{1}{2} \left[-\hat{U}_c \hat{\chi}_c(\mathbf{q}) \hat{U}_c \right. \\
& \left. + 3\hat{U}_s \hat{\chi}_s(\mathbf{q}) \hat{U}_s + \hat{U}_c + \hat{U}_s \right]_{pl\xi\xi'}^{t\xi'q\ell'}
\end{aligned} \tag{5}$$

where $\hat{\chi}_s$ and $\hat{\chi}_c$ are the static spin and charge susceptibility matrices, respectively.

Within the mRPA approximation, the pairing interaction $\Gamma(\mathbf{k}, \mathbf{k}')$ between Cooper pairs at $(\mathbf{k}, -\mathbf{k})$ and $(\mathbf{k}', -\mathbf{k}')$ can be computed from Eq. (5) as [19, 20]

$$\begin{aligned}
\Gamma(\mathbf{k}, \mathbf{k}') = & \text{Re} \sum_{\ell\ell'\xi\xi'} \sum_{pqst} \left[\psi_{\nu_{-\mathbf{k}}}^{t\xi'}(-\mathbf{k}) \right]^* \left[\psi_{\nu_{\mathbf{k}}}^{s\xi*}(\mathbf{k}) \right]^* \\
& \times \Gamma_{s\xi t\xi'}^{plq\ell'}(\mathbf{k} - \mathbf{k}') \psi_{\nu_{\mathbf{k}'}}^{pl}(\mathbf{k}') \psi_{\nu_{-\mathbf{k}'}}^{q\ell'}(-\mathbf{k}')
\end{aligned} \tag{6}$$

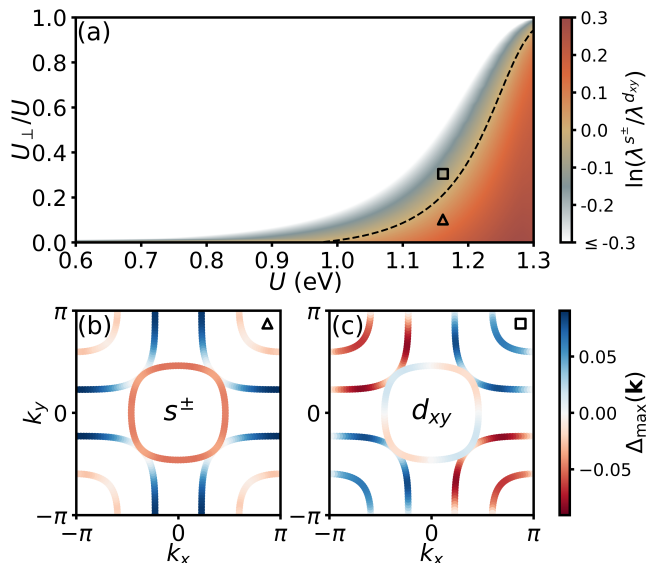


FIG. 2. (a) Phase diagram showing the log of the ratio between the two leading eigenvalues of Eq. (7) for given values of U and U_{\perp} . The corresponding leading gap functions $\Delta_{\max}(\mathbf{k})$ displaying s^{\pm} -wave and d_{xy} -wave symmetries for $U = 1.16$ eV and $U_{\perp}/U = 0.1$ (triangle) and $U_{\perp}/U = 0.3$ (square) are shown in panels (b) and (c), respectively.

where $\psi_{\nu_{\mathbf{k}}}^{p\ell}(\mathbf{k})$ is the $\nu_{\mathbf{k}}$ -th band single-particle electronic state with momentum \mathbf{k} in a basis where p and ℓ are good quantum numbers. The symmetric part of the pairing interaction ($\bar{\Gamma}(\mathbf{k}, \mathbf{k}')$) can, in turn, be used to calculate the gap function $\Delta^{\alpha}(\mathbf{k})$ and the respective pairing strength λ^{α} using the usual integral eigenvalue equation [19]:

$$-\sum_j \oint_{\mathbf{k}' \in C_j} \frac{d\mathbf{k}'_{\parallel}}{v_F(\mathbf{k}')} \frac{1}{(2\pi)^2} \bar{\Gamma}(\mathbf{k}, \mathbf{k}') \Delta^{\alpha}(\mathbf{k}') = \lambda^{\alpha} \Delta^{\alpha}(\mathbf{k}), \quad (7)$$

where the sum runs over the different FS sheets C_j and $v_F(\mathbf{k})$ denotes the Fermi speed at momentum \mathbf{k} .

Superconducting symmetries.— For a given set of parameters entering $\bar{\Gamma}(\mathbf{k}, \mathbf{k}')$, the solution of Eq. (7) with the highest eigenvalue λ_{\max} will correspond to the highest critical temperature T_c and the symmetry of the pairing gap is reflected in the corresponding eigenfunction $\Delta_{\max}(\mathbf{k})$. In the following, we consider the reference value of $U \approx 1.16$ eV, which has been estimated to match $T_c \approx 80$ K [12]. Considering the largest interlayer hopping in the model ($|t_{\perp}^z| \approx 0.635$ eV) [6], this gives a moderate $U/|t_{\perp}^z| \approx 1.83$, reflecting a itinerant electron picture. For these parameters $U_{\perp} = 0$ the leading and sub-leading solutions of Eq. (7) display s^{\pm} -wave and d_{xy} -wave symmetries (with $\lambda^{s^{\pm}}/\lambda^{d_{xy}} > 1$), in accordance with previous studies [8, 11, 14].

For increasing values of U_{\perp} , however, the ratio $\lambda^{s^{\pm}}/\lambda^{d_{xy}}$ decreases and eventually the solution with d_{xy} -wave symmetry becomes dominant. This is illustrated in Figure 2(a), which shows a color map of $\log(\lambda^{s^{\pm}}/\lambda^{d_{xy}})$ for different values of onsite U and interlayer U_{\perp} inter-

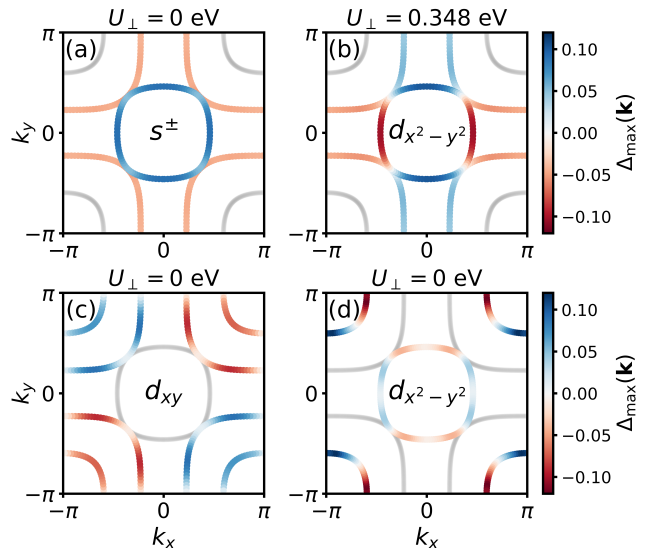


FIG. 3. Color maps of the leading superconducting gap function $\Delta_{\max}(\mathbf{k})$ computed using the two-orbital bilayer pairing vertex but considering only the contributions of two out of the three FS pockets. Panels (a) and (b) shows results excluding the contributions of the γ pocket for $U_{\perp} = 0$ and $U_{\perp} = 0.3U = 0.348$ eV, respectively. Panels (c) and (d) show results for $U_{\perp} = 0$ excluding the contributions of α and β pockets, respectively. In all cases, $U = 1.16$ eV.

action strengths. The dashed line represents the curve $\lambda^{s^{\pm}} = \lambda^{d_{xy}}$ and can be interpreted as a “phase boundary” separating the regions where each gap symmetry dominates.

For the reference value of $U = 1.16$ eV, we find that the transition point occurs at a moderate value of $U_{\perp}^c \approx 0.2U = 0.23$ eV, with the gap functions displaying s^{\pm} -wave and d_{xy} -wave symmetries for $U_{\perp} < U_{\perp}^c$ and $U_{\perp} > U_{\perp}^c$ (Figs. 2(b) and (c)), respectively. For larger values of U , however, the s^{\pm} -wave symmetry is clearly favored even for ratios U_{\perp}/U as large as 50 – 60%.

Some insight as to why the interlayer interaction tends to favor a d-wave symmetry over the s^{\pm} one can be gained by looking more closely on the role of the interorbital contribution to the pairing interaction. Imagine if one could tune the relative contributions of the different FS sheets to the pairing gap function defined by Eq. (7). In practice, this can be done by artificially giving different weights to the terms in the sum on the left-hand-side of Eq. (7). For instance, one could exclude (assign zero weight to) the contribution of one of the FS pockets (α , β , or γ) and see what the resulting symmetry of the leading pairing gap function looks like.

This is done in Fig. 3 for $U = 1.16$ eV. Figure 3(a) shows that, for $U_{\perp} = 0$, the pairing gap symmetry remains s^{\pm} -wave even if the contribution of the γ pocket is excluded and only pockets α and β , which are dominated by $3d_{x^2-y^2}$ orbitals and hence have a more “planar” character, are considered in the calculation. In a sense, this would mimic a “cuprate-like” scenario [16].

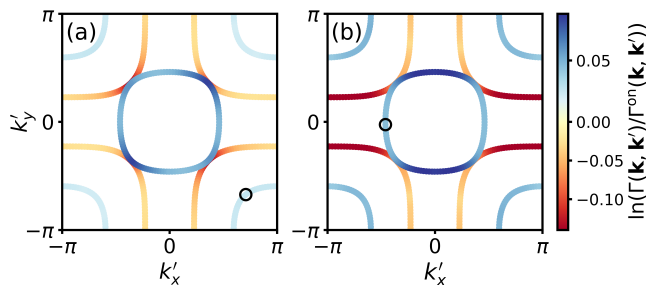


FIG. 4. Enhancement of the pairing vertex function ($\Gamma(\mathbf{k}, \mathbf{k}')$) by interlayer interactions. Panels (a) and (b) show the ratio of $\Gamma(\mathbf{k}, \mathbf{k}')$ calculated with $U_{\perp} = 0.348$ eV and $\Gamma^{\text{on}}(\mathbf{k}, \mathbf{k}')$, calculated with $U_{\perp} = 0$ in a logarithmic scale for a fixed \mathbf{k} (black ring) located at (a) γ and (b) α Fermi surface pockets, dominated by $d_{3z^2-r^2}$ and $d_{x^2-y^2}$ orbitals respectively.

In this situation, by increasing U_{\perp} the symmetry of the leading gap function becomes $d_{x^2-y^2}$ and *not* d_{xy} , as in the case where all pockets are considered (Fig. 2(c)). On the other hand, the pairing symmetry becomes d_{xy} if, instead, the contribution of the α pocket is excluded (Fig. 3(c)). Even though Fig. 3(c) shows results for $U_{\perp} = 0$, we have checked that this result holds for a large range of U_{\perp} values. Finally, if the contribution of the β pocket is excluded, the gap symmetry becomes $d_{x^2-y^2}$ (Fig. 3(d)) and *not* d_{xy} .

These results indicate that, when all three pockets are considered in the calculation (Fig. 2), by increasing U_{\perp} , the relative contribution of the γ pocket (dominated by $3d_{z^2}$ orbitals) increases over the (more planar) α pocket contribution, thereby inducing the switching between s^{\pm} - and nodal d_{xy} -wave pairing symmetries. As such, the interplay between γ and α pockets in the pairing vertex is a crucial element in explaining the $s^{\pm} \rightarrow d_{xy}$ order switching as U_{\perp} increases.

This conclusion is further supported by looking at the differences in the pairing vertex function $\Gamma(\mathbf{k}, \mathbf{k}')$ for $U_{\perp} = 0.348$ eV and $U_{\perp} = 0$. Figure 4 shows the ra-

tio between $\Gamma(\mathbf{k}, \mathbf{k}')$ (calculated with $U_{\perp} = 0.348$ eV) and $\Gamma^{\text{on}}(\mathbf{k}, \mathbf{k}')$ (calculated with $U_{\perp} = 0$), for a fixed \mathbf{k} (marked as a black circle) and as a function of \mathbf{k}' along the FS.

For example, as shown in Fig., 4(a), for a \mathbf{k} -point located in the γ pocket, increasing U_{\perp} leads to an *enhancement* of the pairing vertex function ($\Gamma(\mathbf{k}, \mathbf{k}') > \Gamma^{\text{on}}(\mathbf{k}, \mathbf{k}')$) along the α pocket and a *decrease* ($\Gamma(\mathbf{k}, \mathbf{k}') < \Gamma^{\text{on}}(\mathbf{k}, \mathbf{k}')$) along the β pocket. A similar result occurs when \mathbf{k} is located at the α pocket (Fig, 4(b)): the pairing vertex function is enhanced along the γ pocket and decreases along the β pocket.

This result is consistent with our picture that interlayer interactions tend to favor the d_{xy} pairing symmetry over the s^{\pm} by favoring the interorbital pairing between electrons in the γ and α pockets, which are dominated by the $d_{3z^2-r^2}$ and $d_{x^2-y^2}$ orbital contributions, respectively.

Concluding remarks.— In this work, we investigate the role of interlayer Coulomb interaction terms on the superconducting properties of $\text{La}_3\text{Ni}_2\text{O}_7$ under pressure. Our results indicate that for moderate onsite interactions in the model (up to $U \sim 1.1$ eV), and relatively small interlayer interaction strengths (about $\sim 30\%$ of the onsite term) the leading pairing symmetry becomes of the d_{xy} -wave type instead of the s^{\pm} -wave predicted by several works in the *absence* of interlayer interactions [8, 11, 12, 14–16, 31, 32]. Our calculations also confirm that the s^{\pm} solution is dominant for large onsite interactions ($U \gtrsim 1.3$ eV), which agrees with previous calculations based on $t - J - J_{\perp}$ models [14].

More interestingly, our analysis shows that the superconducting pairing symmetry is strongly dependent on the interplay of *all three* Fermi surface pockets. In particular, the interlayer interaction tends to favor interorbital pairing between electrons with $d_{3z^2-r^2}$ and $d_{x^2-y^2}$ orbital character, underscoring the view that a complete description of the superconducting properties can only be achieved by multi-orbital models [8–10, 16].

We acknowledge financial support from the São Paulo Research Foundation (FAPESP), Brazil (process numbers 2022/15453-0 and 2023/14902-8) and from CNPq (Grant No. 312622/2023-6).

-
- [1] H. Sun, M. Huo, X. Hu, J. Li, Z. Liu, Y. Han, L. Tang, Z. Mao, P. Yang, B. Wang, J. Cheng, D.-X. Yao, G.-M. Zhang, and M. Wang, Signatures of superconductivity near 80 K in a nickelate under high pressure, *Nature* **621**, 493 (2023).
- [2] G. Wang, N. N. Wang, X. L. Shen, J. Hou, L. Ma, L. F. Shi, Z. A. Ren, Y. D. Gu, H. M. Ma, P. T. Yang, Z. Y. Liu, H. Z. Guo, J. P. Sun, G. M. Zhang, S. Calder, J.-Q. Yan, B. S. Wang, Y. Uwatoko, and J.-G. Cheng, Pressure-induced superconductivity in polycrystalline $\text{La}_3\text{Ni}_2\text{O}_{7-\delta}$, *Physical Review X* **14**, 011040 (2024).
- [3] J. Li, P. Ma, H. Zhang, X. Huang, C. Huang, M. Huo, D. Hu, Z. Dong, C. He, J. Liao, X. Chen, T. Xie, H. Sun, and M. Wang, Pressure-driven right-triangle shape superconductivity in bilayer nickelate $\text{La}_3\text{Ni}_2\text{O}_7$, [arXiv , 2404.11369](https://arxiv.org/abs/2404.11369) (2024).
- [4] M. Wang, H.-H. Wen, T. Wu, D.-X. Yao, and T. Xiang, Normal and superconducting properties of $\text{La}_3\text{Ni}_2\text{O}_7$, *Chinese Physics Letters* **41**, 077402 (2024).
- [5] E. K. Ko, Y. Yu, Y. Liu, L. Bhatt, J. Li, V. Thampy, C.-T. Kuo, B. Y. Wang, Y. Lee, K. Lee, J.-S. Lee, B. H. Goodge, D. A. Muller, and H. Y. Hwang, Signatures of ambient pressure superconductivity in thin film $\text{La}_3\text{Ni}_2\text{O}_7$, *Nature* (2024).
- [6] Z. Luo, X. Hu, M. Wang, W. Wú, and D.-X. Yao, Bilayer two-orbital model of $\text{La}_3\text{Ni}_2\text{O}_7$ under pressure, *Physical Review Letters* **131**, 126001 (2023).
- [7] Y. Zhang, L.-F. Lin, A. Moreo, and E. Dagotto, Elec-

- tronic structure, dimer physics, orbital-selective behavior, and magnetic tendencies in the bilayer nickelate superconductor $\text{La}_3\text{Ni}_2\text{O}_7$ under pressure, [Physical Review B **108**, L180510 \(2023\)](#).
- [8] Y. Zhang, L.-F. Lin, A. Moreo, T. A. Maier, and E. Dagotto, Structural phase transition, $s\pm$ -wave pairing, and magnetic stripe order in bilayered superconductor $\text{La}_3\text{Ni}_2\text{O}_7$ under pressure, [Nature Communications **15**, 2470 \(2024\)](#).
- [9] F. Lechermann, J. Gondolf, S. Bötzel, and I. M. Eremin, Electronic correlations and superconducting instability in $\text{La}_3\text{Ni}_2\text{O}_7$ under high pressure, [Physical Review B **108**, L201121 \(2023\)](#).
- [10] Z. Luo, B. Lv, M. Wang, W. Wú, and D.-X. Yao, High-TC superconductivity in $\text{La}_3\text{Ni}_2\text{O}_7$ based on the bilayer two-orbital t-J model, [npj Quantum Materials **9**, 1 \(2024\)](#).
- [11] Q.-G. Yang, D. Wang, and Q.-H. Wang, Possible $s\pm$ -wave superconductivity in $\text{La}_3\text{Ni}_2\text{O}_7$, [Physical Review B **108**, L140505 \(2023\)](#).
- [12] Y.-B. Liu, J.-W. Mei, F. Ye, W.-Q. Chen, and F. Yang, s^\pm -wave pairing and the destructive role of apical-oxygen deficiencies in $\text{La}_3\text{Ni}_2\text{O}_7$ under pressure, [Physical Review Letters **131**, 236002 \(2023\)](#).
- [13] F. Lechermann, S. Bötzel, and I. M. Eremin, Electronic instability, layer selectivity, and fermi arcs in $\text{La}_3\text{Ni}_2\text{O}_7$, [Physical Review Materials **8**, 074802 \(2024\)](#).
- [14] X.-Z. Qu, D.-W. Qu, J. Chen, C. Wu, F. Yang, W. Li, and G. Su, Bilayer $t-J-J_\perp$ model and magnetically mediated pairing in the pressurized nickelate $\text{La}_3\text{Ni}_2\text{O}_7$, [Physical Review Letters **132**, 036502 \(2024\)](#).
- [15] J. Chen, F. Yang, and W. Li, Orbital-selective superconductivity in the pressurized bilayer nickelate $\text{La}_3\text{Ni}_2\text{O}_7$: An infinite projected entangled-pair state study, [Physical Review B **110**, L041111 \(2024\)](#).
- [16] Z. Fan, J.-F. Zhang, B. Zhan, D. Lv, X.-Y. Jiang, B. Normand, and T. Xiang, Superconductivity in nickelate and cuprate superconductors with strong bilayer coupling, [Physical Review B **110**, 024514 \(2024\)](#).
- [17] T. Xie, M. Huo, X. Ni, F. Shen, X. Huang, H. Sun, H. C. Walker, D. Adroja, D. Yu, B. Shen, L. He, K. Cao, and M. Wang, Strong interlayer magnetic exchange coupling in $\text{La}_3\text{Ni}_2\text{O}_7-\delta$ revealed by inelastic neutron scattering, [Science Bulletin **10.1016/j.scib.2024.07.030** \(2024\)](#).
- [18] X. Chen, J. Choi, Z. Jiang, J. Mei, K. Jiang, J. Li, S. Agrestini, M. Garcia-Fernandez, H. Sun, X. Huang, D. Shen, M. Wang, J. Hu, Y. Lu, K.-J. Zhou, and D. Feng, Electronic and magnetic excitations in $\text{La}_3\text{Ni}_2\text{O}_7$, [Nature Communications **15**, 9597 \(2024\)](#).
- [19] S. Graser, T. A. Maier, P. J. Hirschfeld, and D. J. Scalapino, Near-degeneracy of several pairing channels in multiorbital models for the Fe pnictides, [New Journal of Physics **11**, 025016 \(2009\)](#).
- [20] A. F. Kemper, T. A. Maier, S. Graser, H.-P. Cheng, P. J. Hirschfeld, and D. J. Scalapino, Sensitivity of the superconducting state and magnetic susceptibility to key aspects of electronic structure in ferropnictides, [New Journal of Physics **12**, 073030 \(2010\)](#).
- [21] M. Altmeyer, D. Guterding, P. J. Hirschfeld, T. A. Maier, R. Valentí, and D. J. Scalapino, Role of vertex corrections in the matrix formulation of the random phase approximation for the multiorbital Hubbard model, [Physical Review B **94**, 214515 \(2016\)](#).
- [22] G. B. Martins, A. Moreo, and E. Dagotto, Rpa analysis of a two-orbital model for the bis 2 -based superconductors, [Phys. Rev. B **87**, 081102 \(2013\)](#).
- [23] L. B. Braz, G. B. Martins, and L. G. G. V. D. da Silva, Charge and spin fluctuations in superconductors with intersublattice and interorbital interactions, <https://arxiv.org/abs/2403.02453v1> (2024).
- [24] S. Cai, Y. Zhou, H. Sun, K. Zhang, J. Zhao, M. Huo, L. Nataf, Y. Wang, J. Li, J. Guo, K. Jiang, M. Wang, Y. Ding, W. Yang, Y. Lu, Q. Kong, Q. Wu, J. Hu, T. Xiang, H. kwang Mao, and L. Sun, Low-temperature mean valence of nickel ions in pressurized $\text{La}_3\text{Ni}_2\text{O}_7$, [arXiv.org:2412.18343 \(2024\)](#).
- [25] J. Yang, H. Sun, X. Hu, Y. Xie, T. Miao, H. Luo, H. Chen, B. Liang, W. Zhu, G. Qu, C.-Q. Chen, M. Huo, Y. Huang, S. Zhang, F. Zhang, F. Yang, Z. Wang, Q. Peng, H. Mao, G. Liu, Z. Xu, T. Qian, D.-X. Yao, M. Wang, L. Zhao, and X. J. Zhou, Orbital-dependent electron correlation in double-layer nickelate $\text{La}_3\text{Ni}_2\text{O}_7$, [Nature Communications **15**, 4373 \(2024\)](#).
- [26] Y. Li, X. Du, Y. Cao, C. Pei, M. Zhang, W. Zhao, K. Zhai, R. Xu, Z. Liu, Z. Li, J. Zhao, G. Li, Y. Qi, H. Guo, Y. Chen, and L. Yang, Electronic Correlation and Pseudogap-Like Behavior of High-Temperature Superconductor $\text{La}_3\text{Ni}_2\text{O}_7$, [Chinese Physics Letters **41**, 087402 \(2024\)](#).
- [27] Y. Zhang, L.-F. Lin, A. Moreo, T. A. Maier, and E. Dagotto, Electronic structure, magnetic correlations, and superconducting pairing in the reduced ruddlesden-popper bilayer $\text{La}_3\text{Ni}_2\text{O}_6$ under pressure: Different role of $d_{3z^2-r^2}$ orbital compared with $\text{La}_3\text{Ni}_2\text{O}_7$, [Phys. Rev. B **109**, 045151 \(2024\)](#).
- [28] Y. Zhang, L.-F. Lin, A. Moreo, T. A. Maier, and E. Dagotto, Prediction of s^\pm -wave superconductivity enhanced by electronic doping in trilayer nickelates $\text{La}_4\text{Ni}_3\text{O}_{10}$ under pressure, [Phys. Rev. Lett. **133**, 136001 \(2024\)](#).
- [29] The remaining matrix elements can be trivially obtained by exchanging $A \leftrightarrow B$.
- [30] See Supplemental Material at *URL-to-be-inserted* for details, which includes Refs. [6, 19, 33].
- [31] S. Bötzel, F. Lechermann, J. Gondolf, and I. M. Eremin, Theory of magnetic excitations in the multilayer nickelate superconductor $\text{La}_3\text{Ni}_2\text{O}_7$, [Physical Review B **109**, L180502 \(2024\)](#).
- [32] H. Sakakibara, N. Kitamine, M. Ochi, and K. Kuroki, Possible high T_c superconductivity in $\text{La}_3\text{Ni}_2\text{O}_7$ under high pressure through manifestation of a nearly half-filled bilayer hubbard model, [Physical Review Letters **132**, 106002 \(2024\)](#).
- [33] T. Ozaki, Continued fraction representation of the Fermi-Dirac function for large-scale electronic structure calculations, [Physical Review B **75**, 035123 \(2007\)](#).

Supplementary Material for “Interlayer interactions in $\text{La}_3\text{Ni}_2\text{O}_7$ under pressure: from s^\pm to d_{xy} -wave superconductivity”

This Supplementary Material (SM) provides additional information supporting the results in the main text. In Section S1 we demonstrate the details of our model discussed in the section “*Interlayer interactions*” in the main text. In Section S2 we show the pairing symmetries favored by individual Fermi surface pockets as discussed in the section “*Minimal two-orbital model*” in the main text.

S1. MATRIX RANDOM-PHASE APPROXIMATION

Since our investigation focuses on exploring the role of multiorbital effects on the magnetic fluctuations of the pressurized bilayer nickelate, we consider the two-orbital $d_{x^2-y^2}$ and $d_{z^2-r^2}$ low-energy model [6], as represented in Fig. 1(a) of the main text. The non-interacting Hamiltonian reads

$$\begin{aligned}
 H_0 = & \sum_{\mathbf{k}\sigma sS} (T_{\mathbf{k}}^s - \mu) c_{\mathbf{k}sS\sigma}^\dagger c_{\mathbf{k}sS\sigma} \\
 & + \sum_{\mathbf{k}\sigma s} t_\perp^s (c_{\mathbf{k}sA\sigma}^\dagger c_{\mathbf{k}sB\sigma} + \text{h.c.}) \\
 & + \sum_{\mathbf{k}\sigma(s \neq p)S} V_{\mathbf{k}} c_{\mathbf{k}sS\sigma}^\dagger c_{\mathbf{k}pS\sigma} \\
 & + \sum_{\mathbf{k}\sigma(s \neq p)} V'_{\mathbf{k}} (c_{\mathbf{k}sA\sigma}^\dagger c_{\mathbf{k}pB\sigma} + \text{h.c.}),
 \end{aligned} \tag{S1}$$

where $c_{\mathbf{k}sS\sigma}^\dagger$ creates an electron with spin σ , in the orbital $s = \{x, z\}$ corresponding to $\{d_{x^2-y^2}, d_{3z^2-r^2}\}$, sublattice $S = \{A, B\}$, and momentum \mathbf{k} , μ is the chemical potential, and h.c. shortcuts Hermitian conjugate. This model considers up to second-neighbor hoppings such that

$$\begin{aligned}
 T_{\mathbf{k}}^s &= 2t_1^s (\cos k_x + \cos k_y) + 4t_2^s \cos k_x \cos k_y + \epsilon^s \\
 V_{\mathbf{k}} &= 2t_3^{xz} (\cos k_x - \cos k_y), \\
 V'_{\mathbf{k}} &= 2t_4^{zz} (\cos k_x - \cos k_y).
 \end{aligned} \tag{S2}$$

The hopping parameters are given in Ref. [6]. Fig. 1(c) of the main text shows the band structure with its respective orbital composition. There is an interplay between the two orbitals $d_{x^2-y^2}$ (red) and $d_{3z^2-r^2}$ (blue) along the path $\Gamma - \mathbf{X} - \mathbf{M}$. Also, the γ pocket is dominated by the $d_{3z^2-r^2}$ orbital and contributed by a nearly flat hole pocket centered at the \mathbf{M} point.

We consider interactions through a degenerate Hubbard model including interlayer interactions. Within this model, the electrons are not constrained to be localized and the specific values of the interaction strengths are not restricted to the limit $U/t \gg 1$ such as the $t - J$ -like models considered in the previous literature. In fact, it has been estimated using the random-phase approximation within mean-field theory that $U \approx 1.16$ eV to match $T_c = 80$ K [?], while the largest hopping is $t_\perp^z \approx -0.635$ eV [6] such that $U/t_\perp^z \approx -1.83$, which is a moderate value. The interaction Hamiltonian for the two-orbital itinerant electron model is given in the main text. Since we are interested in the magnetic fluctuations caused by interacting electrons, we focus our study on the bare and interacting susceptibilities. Having in mind that the present non-interacting model [Eq. (S1)] is independent of the spin directions, the bare susceptibility is the same for charge or spin channels and can be defined as [19]

$$[\hat{\chi}]_{sCtD}^{pAqB}(\mathbf{q}, i\nu_m) = \int_0^{1/T} d\tau e^{i\nu_m \tau} \langle T_\tau \mathbf{S}_{pAqB}(-\mathbf{q}, \tau) \cdot \mathbf{S}_{sCtD}(\mathbf{q}, 0) \rangle, \tag{S3}$$

where $i\nu_m$ denotes bosonic frequencies, τ imaginary time, T temperature, and T_τ time-ordering. We compute the bare susceptibility in the Green’s function form performing the Matsubara summation numerically using Ozaki’s method [33]. The formalism reads

$$[\hat{\chi}]_{sCtD}^{pAqB}(\mathbf{q}, i\nu_m) = -\frac{T}{N} \sum_{\mathbf{k}i\omega_n} G_{sCpA}(\mathbf{k}, i\omega_n) G_{qBtD}(\mathbf{k} + \mathbf{q}, i\omega_n + i\nu_m), \tag{S4}$$

where

$$G_{sCPA}(\mathbf{k}, i\omega_n) = \sum_{\nu_{\mathbf{k}}} \frac{\psi_{\nu_{\mathbf{k}}}^{sC}(\mathbf{k}) \psi_{\nu_{\mathbf{k}}}^{pA*}(\mathbf{k})}{i\omega_n - E_{\nu_{\mathbf{k}}}(\mathbf{k})}, \quad (\text{S5})$$

and $\psi_{\nu_{\mathbf{k}}}^{sC}(\mathbf{k})$ are non-interacting electron eigenfunctions related to the $\nu_{\mathbf{k}}$ -th $E_{\nu_{\mathbf{k}}}(\mathbf{k})$ energy band of Eq. (S1). We adopt $T = 0.02$ eV.

Within the mRPA, adding the onsite and interlayer interactions reduces to performing a matrix operation such that the spin and charge susceptibilities become

$$\hat{\chi}_s(\mathbf{q}, i\nu_m) = \hat{\chi}(\mathbf{q}, i\nu_m) [\hat{1} - \hat{U}_s \hat{\chi}(\mathbf{q}, i\nu_m)]^{-1}, \quad (\text{S6})$$

$$\hat{\chi}_c(\mathbf{q}, i\nu_m) = \hat{\chi}(\mathbf{q}, i\nu_m) [\hat{1} + \hat{U}_c \hat{\chi}(\mathbf{q}, i\nu_m)]^{-1}. \quad (\text{S7})$$

S2. PAIRING SYMMETRY OF INDIVIDUAL POCKETS

As discussed in Sec. *Superconducting symmetries* of the main text, the role of considering a two-orbital model for the superconductivity of bilayer nickelates can be tested by solving the eigenvalue Eq. (7) for the desired pockets only. In the argumentation, we note that we have checked that no individual pocket shows the desired s^{\pm} - and d_{xy} -wave interplay as the two-orbital model. The calculations are shown in Fig. S1. Panels (a) and (b) show no change in the d_{xy} symmetry of the β pocket as the interlayer coupling varies from $U_{\perp}/U = 0$ (a) to $U_{\perp}/U = 0.3$ (b). In fact, the interlayer interactions do not change the symmetry in any three cases explored. As shown in panel (c), a $d_{x^2-y^2}$ -wave dominates pairing of individual γ pocket, and a g -wave symmetry is obtained for the α pocket alone (d).

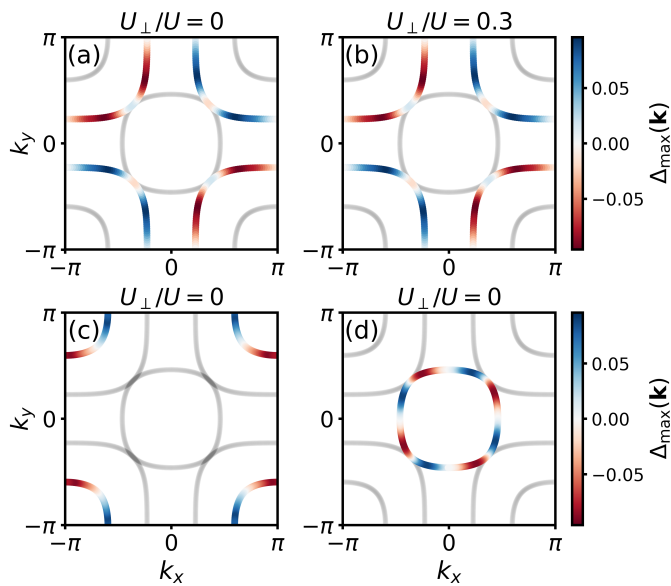


FIG. S1. Same as Fig. 3 of the main text but for individual pockets β (a,b), γ (c), and α (d).

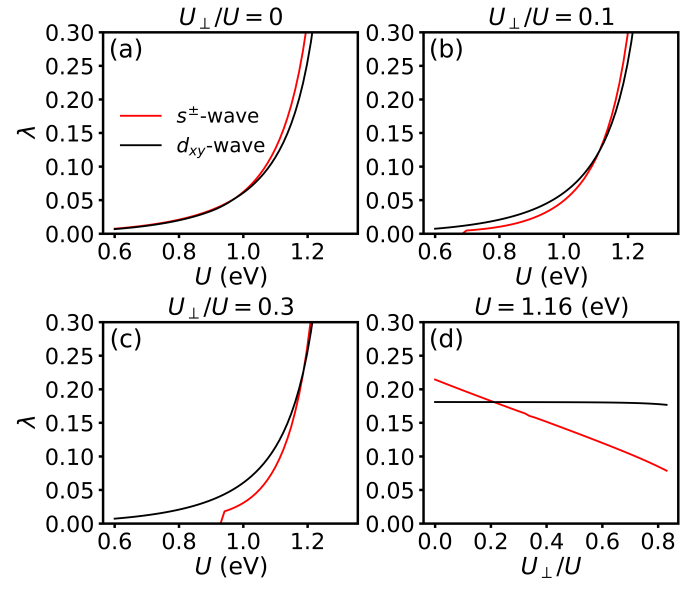


FIG. S2. Cuts of the phase diagram shown in Fig. 2 in the main text.